SUPERCONDUCTING QUANTUM DETECTOR FOR FAR INFRARED ASTRONOMY

Alexei Semenov[1], Heinz-Wilhelm Hübers[1], Andreas Engel[1], and Gregory Gol`tsman[2]

[1]DLR Institute of Space Sensor Technology, Rutherfordstraße 2, 12489 Berlin, Germany
[2]State Pedagogical University, M. Pirogovskaya 29, 119891 Moscow, Russia

ABSTRACT

We present the concept of the superconducting quantum detector for astronomy. Response to a single absorbed photon appears due to successive formation of a normal spot and phase-slip-centres in a narrow strip carrying sub-critical supercurrent. The detector simultaneously has a moderate energy resolution and a variable cut-off wavelength depending on both the material used and operation conditions. We simulated performance of the background-limited direct detector having the 100-micrometer cut-off wavelength. Low dark count rate will allow to realise 10^{-21} W $Hz^{-1/2}$ noise equivalent power at 4 K background radiation. The detection mechanism provides a moderate 1/20 energy resolution at 50-micrometer wavelength.

INTRODUCTION

On-going development of the radiation sensor technology and continuously growing understanding of the Universe provoke challenging astronomical observation projects, which rely on detectors with more and more advanced performance. Future astronomy missions will require detectors having background limited sensitivity in the infrared and submillimeter spectral range even when exposed to relatively weak background radiation. Although the photon counting regime is by definition the one having ultimate sensitivity, integrating direct detectors are traditionally considered for astronomical applications. That is constrained by the near infrared cut-off wavelength of available superconducting[1] and semiconductor[2] photon counters. We have recently proposed[3] a single-photon detection mechanism in a current carrying superconducting film that may become a basis for the novel superconducting quantum detector (SQD) meeting requirements of astronomic applications. The mechanism of the photon detection is the following. A photon absorbed in the superconducting film creates growing normal spot that forces the current to bypass the absorption site. When the current density in the superconducting areas reaches the critical value, the film switches into the resistive state and generates a voltage pulse. Operation of the NbN photon counter has been recently demonstrated[4]. Both theoretical estimate and extrapolation of experimental data show, however, that the NbN counter will have a near-infrared cut-off wavelength for the single-photon detection regime. Implementation of low-transition-temperature superconducting materials will shift the cut-off wavelength towards the submillimeter range, while keeping the ultimate sensitivity. Here we present performance simulations of the Ti based SQD for astronomy.

OPERATION PRPINCIPLE

The key element of the superconducting quantum detector is a narrow superconducting strip biased along its length by subcritical current. Once a photon is absorbed at some point in the strip, there appears a high-energy electron, which then shares its energy with low-energy electrons by means of electron-electron and electron-phonon interaction. The process is commonly called avalanche multiplication, since the number of

Contact information for A. Semenov: Email: Alexei.Semenov@dlr.de, phone (49) 30 670 55 505

low-energy nonequilibrium electrons exponentially grows in time. The maximum number of nonequilibrium electrons appearing in the film per one absorbed photon is referred to as quantum yield or intrinsic quantum efficiency. This figure varies in proportion to the ratio of the quantum energy $h\nu$ and the superconducting energy gap Δ. At any point in the film, the concentration of nonequilibrium electrons increases due to multiplication and decreases due to out-diffusion. Once the concentration has exceeded the equilibrium value specific for the normal state at the superconducting transition temperature, nonequilibrium electrons suppress the energy gap and destroy superconductivity. Consequently, there appears a normal spot centered at the point where the photon has been absorbed. The supercurrent tends to flow around the spot through the still superconducting portion of the film. Fig. 1 illustrates this scenario. With the increase of the spot size the current density in the superconducting sidewalks increases and reaches the critical value. At this very moment a normal, resistive, domain is formed that occupies the cross-section area of the film and gives rise to a voltage pulse with a magnitude proportional to both the resistance of the domain and the bias current. Thus, photon detection occurs due to the joint, collaborative effect of the bias current and growing normal domain.

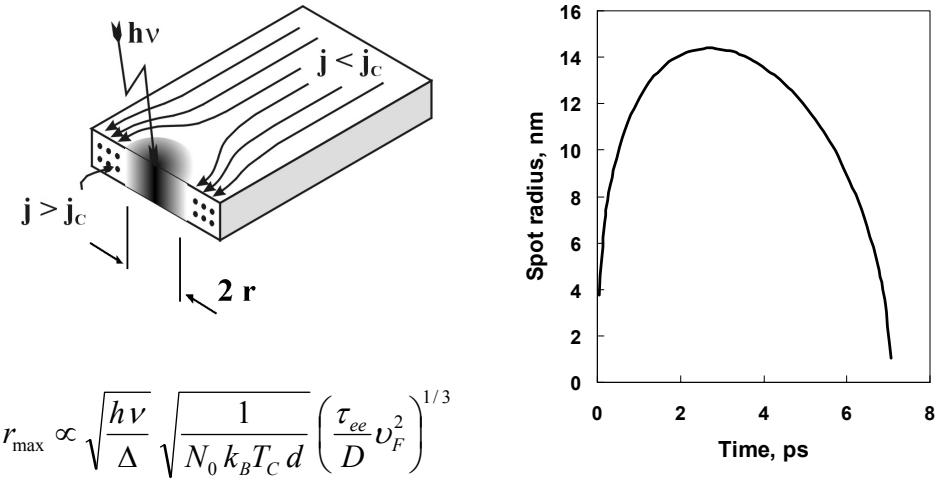

$$r_{\max} \propto \sqrt{\frac{h\nu}{\Delta}} \sqrt{\frac{1}{N_0 k_B T_C d}} \left(\frac{\tau_{ee}}{D} \upsilon_F^2 \right)^{1/3}$$

Figure 1: *Redistribution of the bias current around the normal spot in a thin superconducting film after absorption of photon(upper left). Radius of the spot as function of time (right). Simulations were performed for a 10-nm thick NbN film kept at 0.5 T_C. The expression in the left low corner shows how the maximum radius of the spot depends on material parameters.*

The ability of the SQD to register a single photon with specific energy is the trade-off between the film cross-section, bias current I in comparison with the critical current I_C, and intrinsic quantum efficiency $h\nu/\Delta$. In particular, for a film whose thickness d is much smaller than its width w, the response appears if the diameter of the normal spot exceeds at any moment the value $w(1-I/I_C)$. The expression incorporated in Fig. 1 shows how the maximum spot radius depends on material parameters, i.e. electron density of states N_0, diffusivity D, electron-electron interaction time τ_{ee}, and the Fermi velocity υ_F. Since the intrinsic quantum efficiency drops with the decrease of the quantum energy, there is a material dependent cut-off wavelength for the above described detection mechanism. On the other hand, the intrinsic quantum efficiency turns to be larger in a superconducting material with smaller transition temperature, since it has a smaller energy gap. Thus, for a material with smaller transition temperature the cut-off shifts towards longer wavelengths. The computed cut-off wavelength is shown in Fig. 2 for Ti and NbN films in a range of bias current and strip width. The film thickness 5 nm and the operation temperature 0.5 T_C were assumed for both materials. According to our estimate, a detector from titanium should provide at least an order of magnitude larger cut-off wavelength than NbN photon counters.

The life time of the normal spot drops when the energy deposited by the photon decreases. This provides the basis for energy resolution. However, bias current deteriorates energy resolution if dissipated Joule energy proves to be comparable or larger than the photon energy. Quick feed-back in the voltage bias regime should be able to minimize this effect.

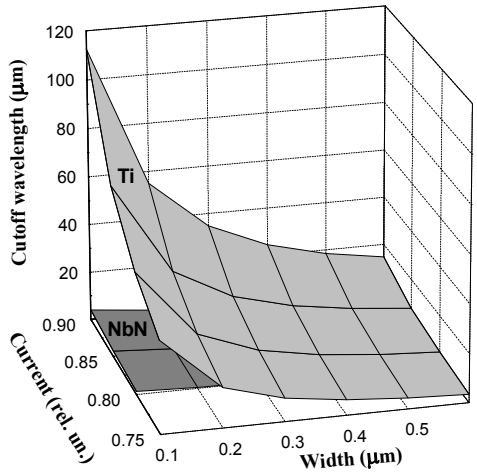

Figure 2: *Cutoff wavelength for NbN and Ti quantum detectors. Bias current is plotted in units of the critical current at the operation temperature* (0.5 T_C).

QUANTUM DETECTOR FOR ASTRONOMY

We simulate major figures of merit for the detector from superconducting titanium film making use of the model described in Ref. 3. We assume that films have the density of states $6.8 \cdot 10^{24}$ $m^{-3} K^{-1}$ of bulk titanium and the BCS energy gap. The electron-electron interaction time at the Fermi level is calculated in the extreme dirty limit using recently reported[5] resistivity $2 \cdot 10^{-6}$ Ω m and 1.6-K transition temperature of Ti films. The electron diffusivity was concluded from the Lorentz number, resistivity, and the value of the Sommerfeld constant $6.8 \cdot 10^{-4}$ J $cm^{-3} K^{-2}$ for bulk titanium. We suggest the 100-μm cut-off wavelength. That is we assume (see Fig. 2) the operation temperature 0.5 T_C, film thickness 5 nm, film width 100 nm, and the bias current 0.9 I_C. Using these parameters and taking into account self-heating, we estimated the response duration ≈ 1 ns for 70-μm wavelength photons.

In order to have significant coupling with radiation, the detector should be integrated into a planar antenna or form a meander-line covering an area larger than squared wavelength. We suggest that the detector be incorporated with a typical terahertz antenna[6] that has a frequency independent optical coupling efficiency of −10 dB and diffraction limited pattern with a 6-mm effective aperture. The frequency band of the antenna should encompass the cut-off frequency of the detector. Since the inner terminals of the feed antenna must be smaller than one tenth of the wavelength in the supporting dielectric, the detector should have a submicron length. We choose for simulation the detector length 0.3 μm. In order to prevent switching of the strip into the normal state, the difference between the critical current and the bias current should be noticeably larger than fluctuations of the critical current value. For such biases the detector noise appears as random voltage pulses (dark counts), which are indistinguishable from those caused by absorbed photons. The origin of dark counts is the fluctuations of the order parameter in the film. We scaled the dark count rate measured for NbN quantum detectors[4] to obtain the mean dark count rate ≈ 10^2 sec^{-1} for Ti detector at 0.6 K biased by 0.9 I_C. The same count rate would be produced by the black body background with a temperature of 6.3 K. Corresponding background limited NEP will be $1.6 \cdot 10^{-19}$ W $Hz^{-1/2}$. Further decrease of the background radiation intensity does not lead to a better performance, since NEP is limited by dark counts. Estimated response duration of 1 ns defines the 42-K temperature of the saturating black body background. At this background the NEP will be $1.8 \cdot 10^{-15}$ W $Hz^{-1/2}$.

Fig. 3 shows the simulated noise equivalent power of the Ti SQD for a set of bias currents and optical coupling efficiencies. All curves have a plateau at small background temperatures corresponding to dominance of the dark counts. When the background count rate exceeds the dark count rate, NEP starts to

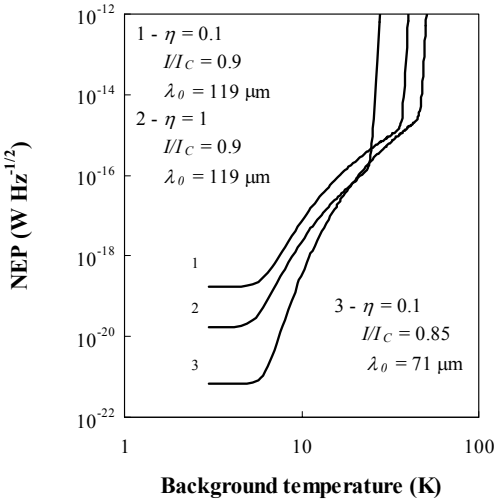

Figure 3: *Noise equivalent power of Ti SQD exposed to blackbody background for different bias currents (I/I_C) and optical coupling efficiencies (η), λ_0 is the cutoff wavelength.*

increase with the background temperature. Step like increase of NEP at larger temperatures corresponds to the transition of the detector to the normal state. Decrease of the bias current to 0.85 I_C shifts the cut-off wavelength to ≈ 70 μm and lowers the dark count rate that results in a better NEP. Projected performance of our detector appears better than that of commonly used stressed Ge:Ga detectors[7], which typically have background limited NEP of about 10^{-18} W Hz$^{-1/2}$. In order to compare our detector with alternative hot-electron bolometer detectors, we specify also the noise equivalent power transformed to the device input. Setting the optical coupling $\eta = 1$ (see curve 2 in Fig. 3), we obtain the background limited NEP $1.6 \cdot 10^{-20}$ W Hz$^{-1/2}$ for 4-K blackbody background. Another advantage of the proposed SQD is the intrinsic energy resolution. We estimated for our detector statistically limited resolution of ≈ 1 meV FWHM for 70-μm (18 meV) photons. Although this figure will be hampered by electronic noise, we believe that it remains sufficient for low-resolution far-infrared spectroscopy, e.g. spectroscopy of interstellar dust clouds[8].

REFERENCES

1. P. Verhoeve, N Rando, A. Peacock, A. van Dordrecht, A. Poelaert, and D.J. Goldie, IEEE Transactions on Applied Superconductivity **7**, 3359 (1997).
2. S. Takeuchi, J. Kim, Y. Yamamoto, H.H. Hogue, APL **74**, 1063 (1999).
3. A.D. Semenov, G.N. Gol'tsman, and A.A. Korneev, Physica C **351**, 349 (2001).
4. G. Gol'tsman, O. Okunev, G. Chulkova, A. Lipatov, A. Semenov, K. Smirnov, B. Voronov, A. Dzardanov, C. Williams, and R. Sobolewski, APL **79**, 705 (2001).
5. G. Gol'tsman, A. Semenov, K. Smirnov, and B. Voronov, Proceedings of the 12th International Symposium on Space Terahertz Technology, San Diego, February 2001, (Pasadena, CA, California Institute of Technology), pp. 469-475.
6. A.D. Semenov, H.-W. Hübers, J. Schubert, G.N. Gol'tsman, A.I. Elantiev, B.M. Voronov, and E.M. Gershenzon, Journal of Applied Physics **88**, 6758 (2000).
7. J. Wolf, R. Katterlocher, D. Lemke, U. Grözinger, L. Hermans, O. Frenzl, D. Engemann, J, Beeman, and M. Fabbricotti, Proceedings of the 30th ESLAB Symposium on Submillimeter and Far-Infrared Space Instrumentation, pp. 25-28, September 1996, Noordwijk, The Netherlands.
8. G. B. Heim, M. L. Henderson, K. MacFeely, T. J. McMahon, D. Michika, R. J. Pearson, G. H. Rieke, J. P. Schwenker, D. W. Strecker, C. Thompson, R. M. Warden, D. A. Wilson, and E. T. Young", MIPS Report 1996 (http://mips.as.arizona.edu/MIPS/Instrument_f.html).